***New Phytologist* Supporting Information**

Article Title: **Rab-E and its interaction with myosin XI are essential for polarized cell growth**

Authors: Robert G. Orr, Fabienne Furt, Erin L. Warner, Erin M. Agar, Jennifer M. Garbarino, Sarah E. Cabral, Michelle L. Dubuke, Allison M. Butt, Mary Munson, and Luis Vidali

Article acceptance date: 12 October 2020.

The following Supporting Information is available for this article:

Fig. S1 Subcellular localization of Rab-E12 and independent Rab-E14 lines.

Fig. S2 Sequence alignment of *P. patens* Rab-E and phylogenetic tree of - and Rab-E-like proteins.

Fig. S3 CRISPR/Cas9 knockout of Rab-E14 and Rab-E15.

Fig. S4 Rab-E sequence conservation and prediction of Myosin XI-CBD and GTP-bound Rab-E14 binding interface.

Fig. S5 Ramachandran plots and average RMSDs for myoXIa-CBD and Rab-E14 homology models

Fig. S6 A structure-based sequence alignment of myoXIa-CBD homology model and myo2p-CBD crystal structure.

Fig. S7 Detection of myosin XI protein abundance in Y2H experiments

Fig. S8 Myosin XI cargo-binding domain mutants show varying levels of solubility

Methods S1 Experimental procedures for supplemental figures

Table S1 Primers used in this study.

Table S2 Gene IDs and source of protein sequences used in phylogenetic tree construction.

Video S1 Confocal live-cell imaging of apical caulonemal cell growth in the 3xmCherry-Rab-E14 and MyosinXIa-3xmEGFP transgenic line.

Video S2 Confocal live-cell imaging of apical caulonemal cell growth in the 3xmEGFP-Rab-E12 transgenic line.

Video S3 Confocal live-cell imaging of cell division in the 3xmCherry-Rab-E14 and MyosinXIa-3xmEGFP transgenic line.

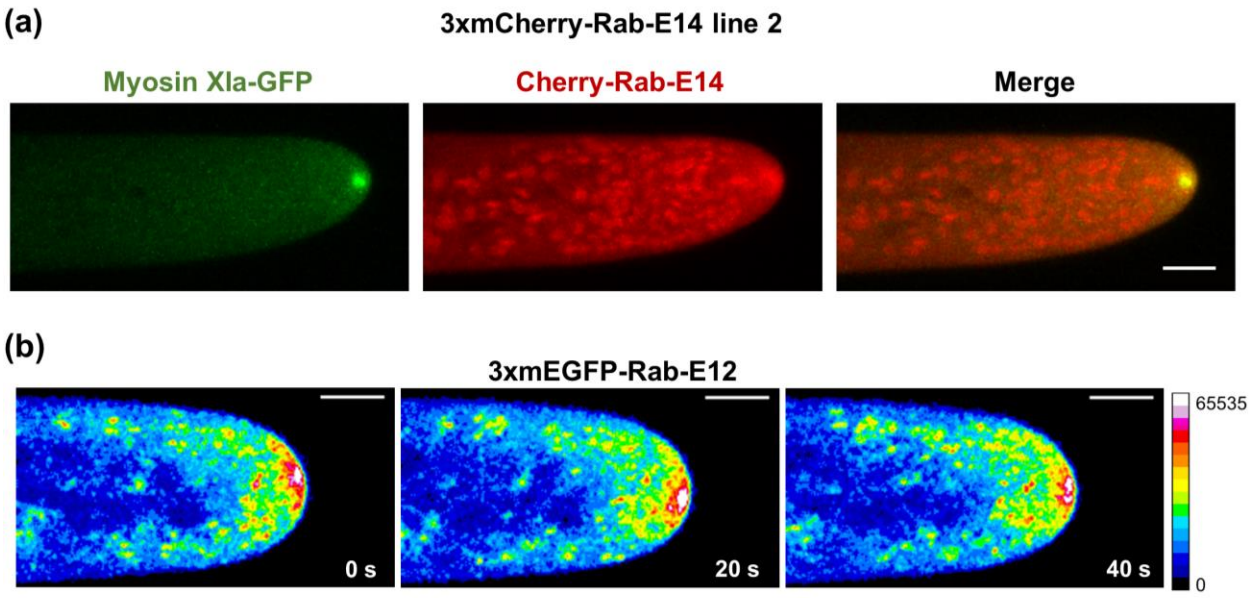

Fig. S1 Subcellular Localization of Rab-E12 and Independent Rab-E14 Lines. (a) Subcellular localization of 3xmEGFP-Rab-E12 by confocal microscopy. Images are maximum projections of 3 confocal slices to visualize the medial volume of the cell and acquired at 5-sec intervals. Selected images from a time series are shown using a 16-color look-up table with the corresponding pixel value range shown on the right. (b) Subcellular localization of 3xmCherry-Rab-E14 and MyosinXIa-3xmEGFP from an independently isolated line. Scale bar, 5 µm

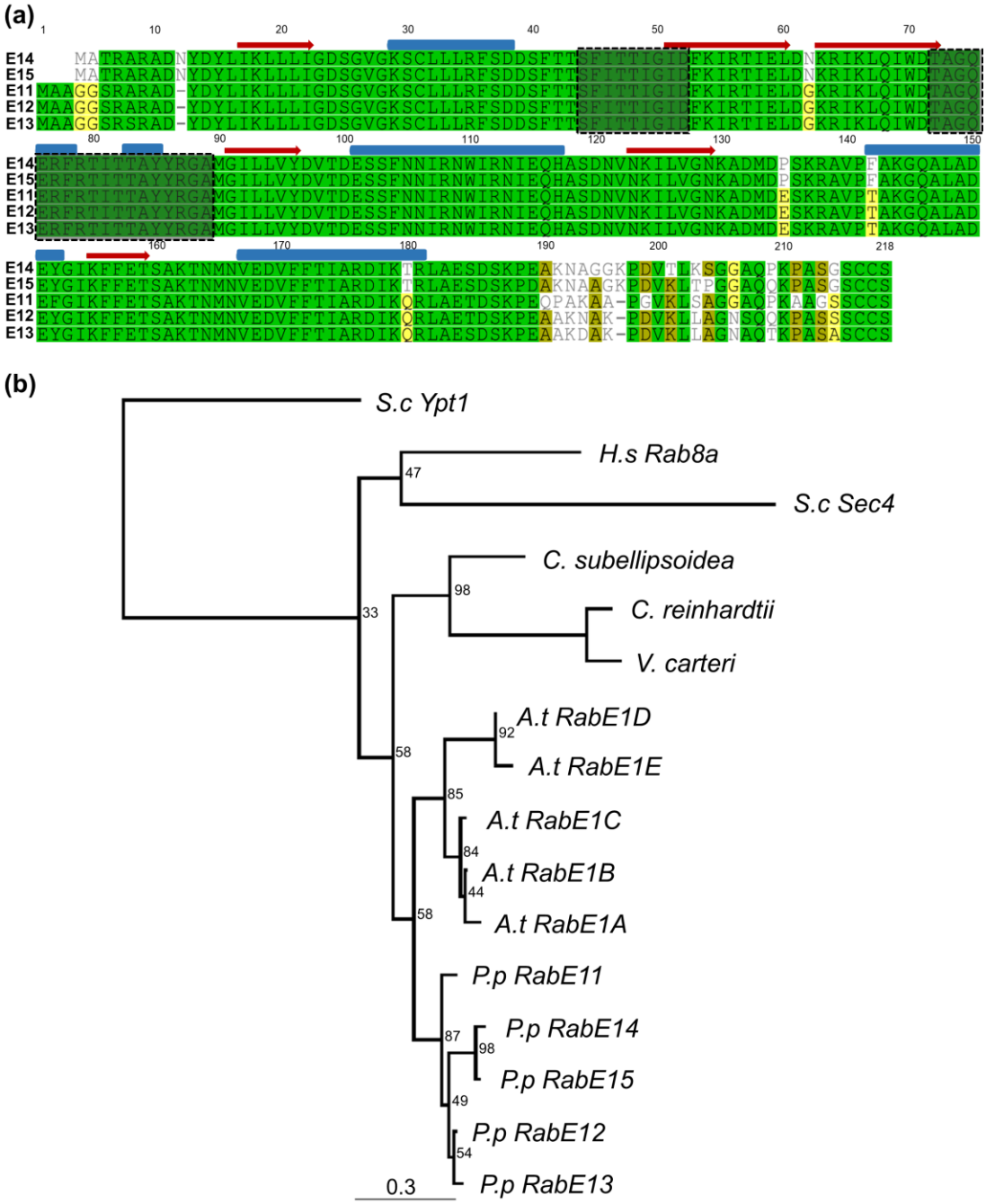

Fig. S2 Sequence alignment of *P. patens* RabE and phylogenetic tree of Rab-E and Rab-E-like proteins. (a) Multiple sequence alignment of the five members of the *Physcomitrella patens* Rab-E subfamily. Pairwise percent identity ranges from 89% (Rab-E14:Rab-E11), to 97% (Rab-E14:Rab-E15, Rab-E12:Rab-E13). Pairwise residue percent similarity is visualized by color: green=100%, yellow=60-80%, white<60%. Predicted secondary structure of active RabE14—red arrow=β-sheet, blue tube=α-helix. Switch I and II domains are outlined by the dotted line. (b) Maximum likelihood phylogenetic tree of RabE subfamily members from select *Viridiplantae* species (*Coccomyxa subellipsoidea, Chlamydomonas reinhardtii, Volvox carteri, Arabidopsis thaliana, Physcomitrella patens*) and homologous Rab8a from human and Sec4 from *Saccharomyces cerevisiae*. *Saccharomyces cerevisiae* Ypt1 (Rab1) was used as the outgroup. Numbers indicate bootstrap support values for their respective branch.

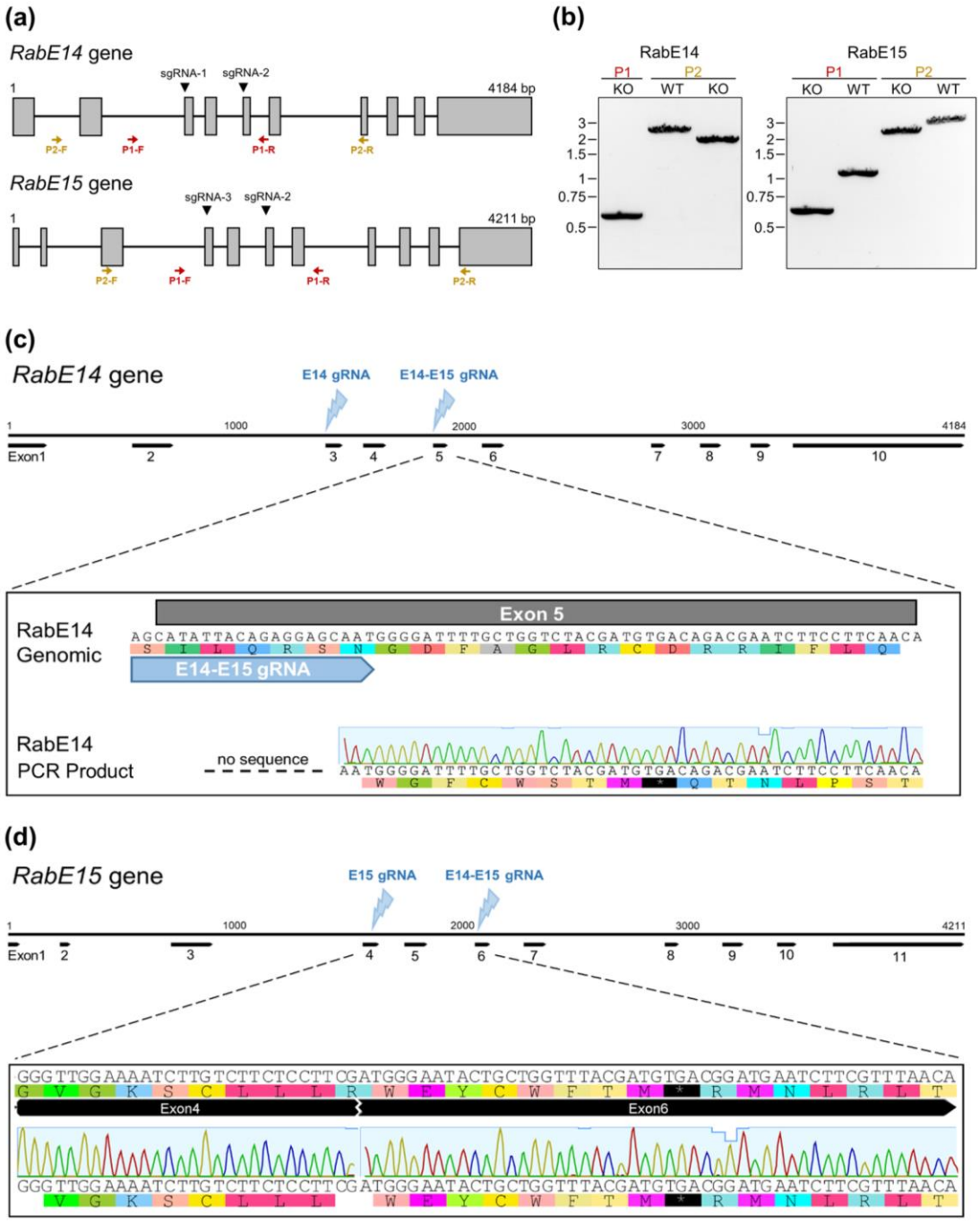

Fig. S3 CRISPR/Cas9 knockout of Rab-E14 and Rab-E15. (a) Schematic of the Rab-E14 and Rab-E15 genomic loci that were targeted for CRISPR-mediated knockout. For both Rab-E14 and Rab-E15, two sites were targeted with sgRNAs to excise a large fragment from each locus. The gray boxes represent exons, with the arrows underneath showing the location of the primers used for genotyping. (b) Genotyping of the Rab-E14 + Rab-E15 CRISPR knockout line using the primer combinations shown in (a). Both loci show the predicted ~1kb excision indicating successful CRISPR editing with both pairs of sgRNAs. (c) Sequence verification of a premature stop codon located within wild-type exon 5. This Rab-E14 mutation results in a 31-residue protein product. (d) Sequence verification of a premature stop codon located within wild-type exon 6. This Rab-E15 mutation results in a 40-residue protein product.

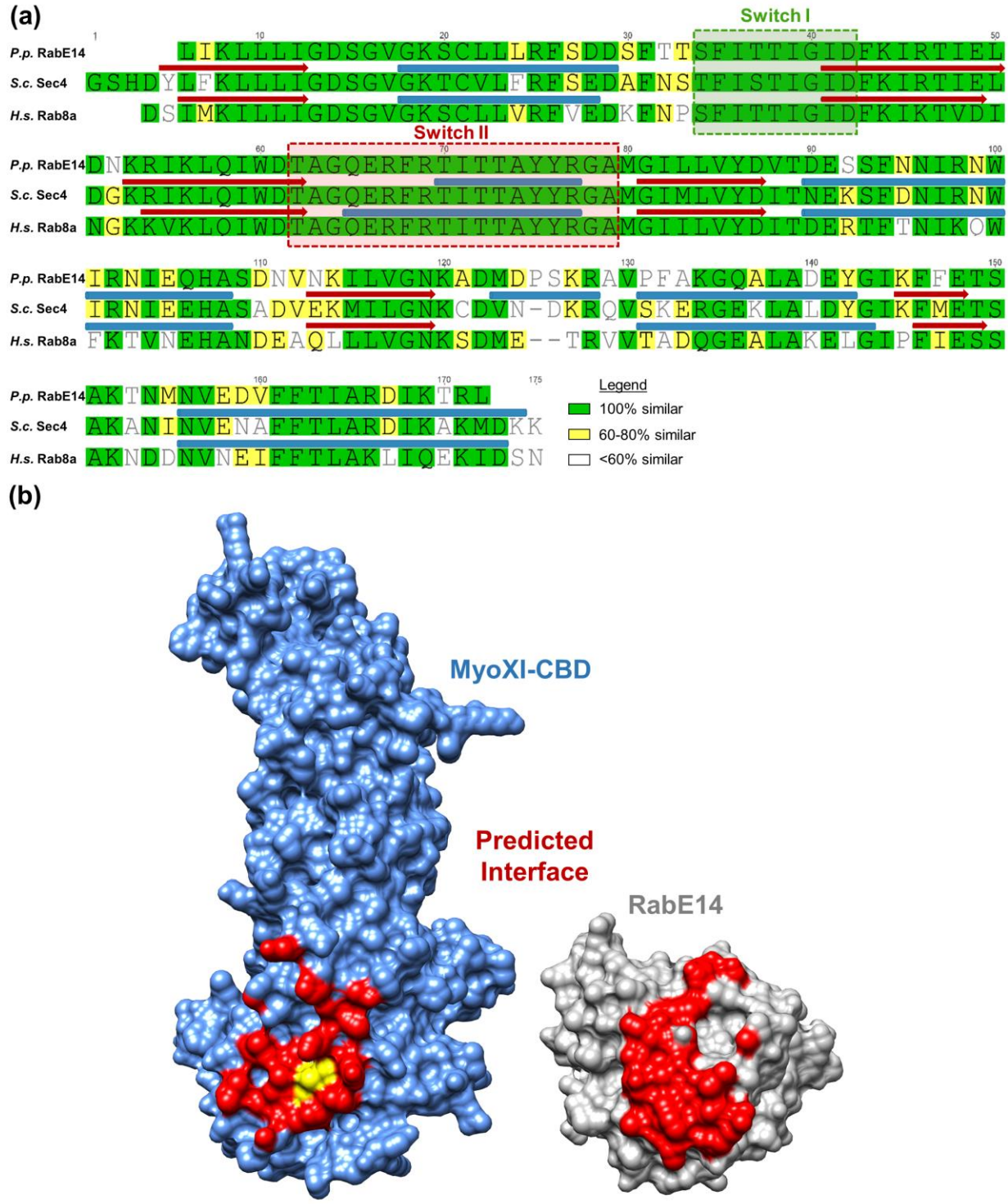

Fig. S4 Rab-E sequence conservation and prediction of Myosin XI-CBD and GTP-bound RabE14 binding interface. (a) Multiple sequence alignment of *Physcomitrella patens* (P.p.) RabE14, *Saccharomyces cerevisiae* (S.c.) Sec4, and *Homo sapiens* (H.s.) Rab8a. Secondary structure (red arrow=β-sheet, blue tube=α-helix) of Sec4 and Rab8a was manually annotated based on their crystal structures, PDB IDs 1G17 and 4LHW, respectively. (b) Predicted MyoXI:RabE interface using homology modeling and structural superposition as described in methods. Modeled contact residues are colored red, with residue V1422 colored yellow.

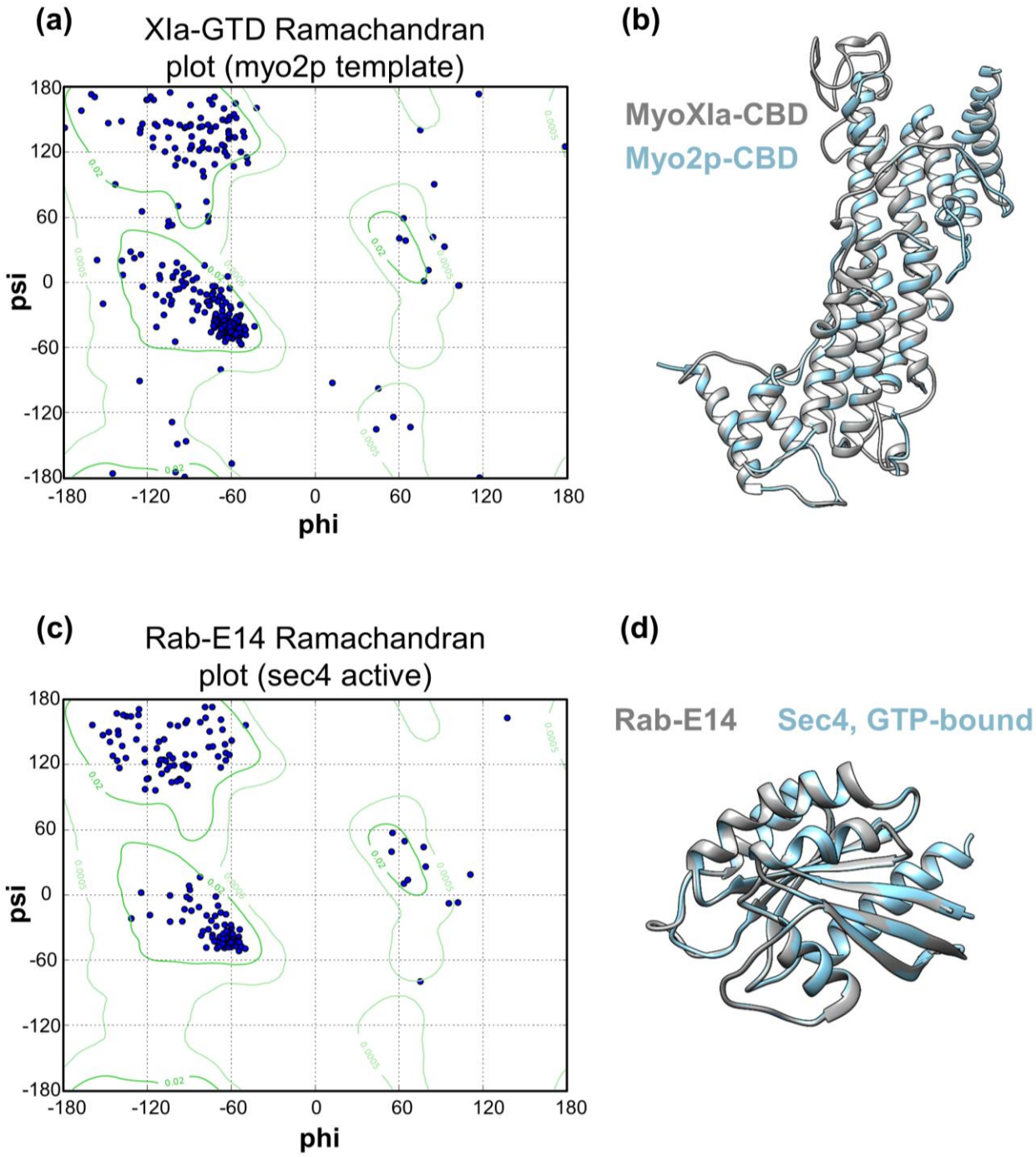

Fig. S5 Ramachandran plots and average RMSDs for myoXIa-CBD and Rab-E14 homology models. (a-d) Both myoXIa-CBD and Rab-E14 homology models used for interface prediction exceed the conventional cutoff of >95% of all non-glycine residues must occupy the energetically allowed regions within the Ramachandran map to conclude good stereochemical quality. (a) Eight non-glycine residues of myoXIa-CBD are located outside of these regions (corresponding to ~98% within). (b) The average RMSD of myoXIa-CBD is 0.291 Å. (c) Four non-glycine residues of GTP-bound Rab-E14 are located outside (corresponding to ~98% within). (d) The average RMSD of GTP-bound Rab-E14 is 0.134 Å

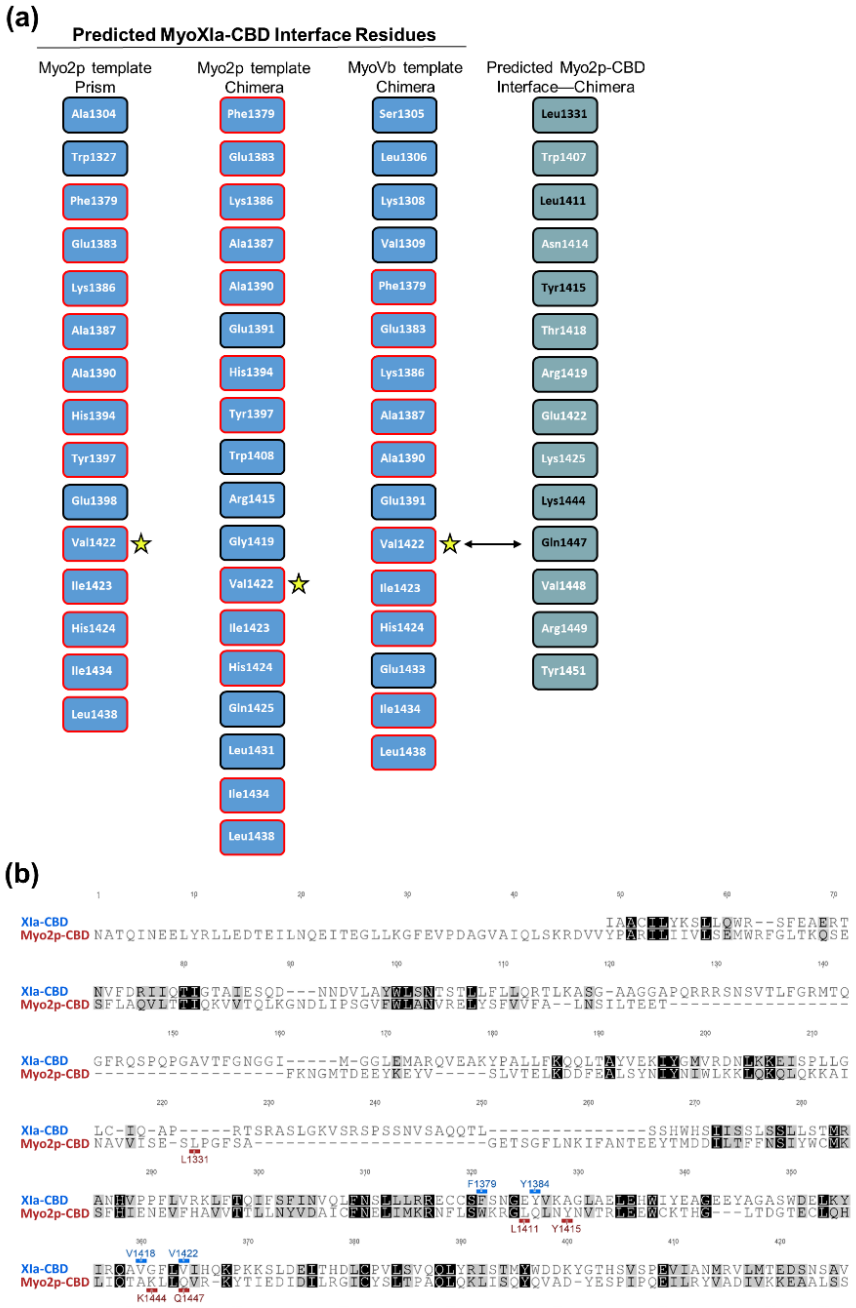

Fig. S6. Prediction of Myosin XI-CBD and GTP-bound Rab-E14 binding interface is robust. (a) Predicted interface residues for MyoXI-CBD using different templates and methods results in similar interface profiles. All interface residues shared between each condition are bordered in red. Importantly, V1422 (star) was shared between all interface predictions and aligns with known interaction residue Q1447 from S.c. Myo2p (shown below). All experimentally identified yeast Myo2p interaction residues, shown in black letters, were captured with structural superposition as described in methods. (b) A structure-based sequence alignment of myoXIa-CBD homology model and myo2p-CBD crystal structure. Structure-based sequence alignment was performed using UCSF Chimera using our homology model of *P. patens* myosin XI cargo-binding domain and crystal structure of *S. cerevisiae* myosin V cargo-binding domain (myo2p-CBD), PDB=2f6h.

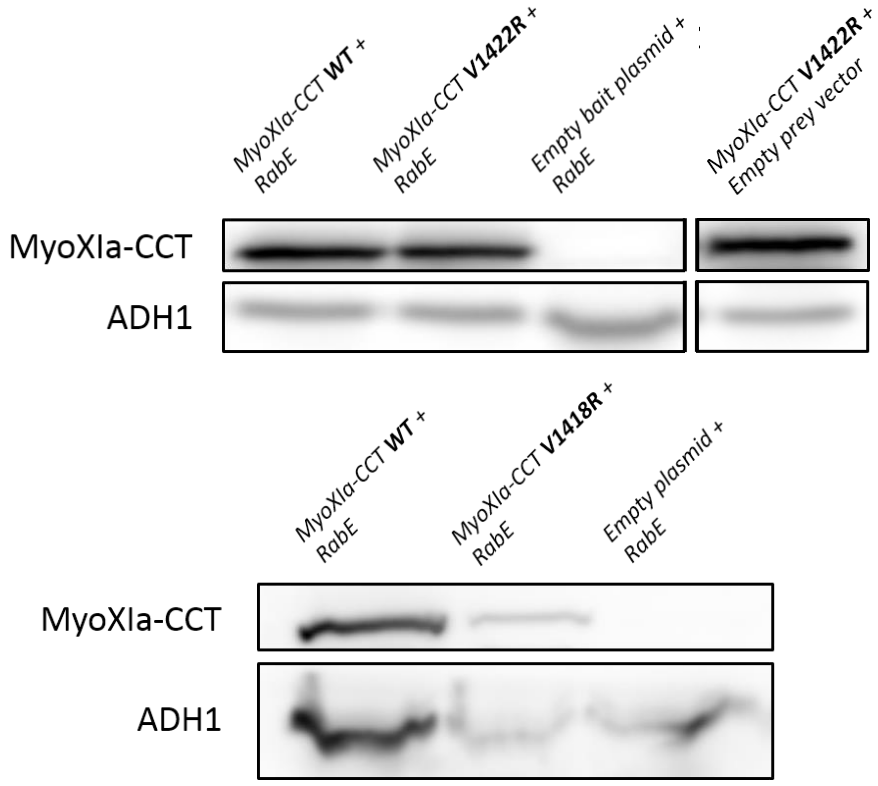

Fig. S7 Detection of myosin XI protein abundance in Y2H experiments. Strains were grown in SD medium lacking trp and leu to an OD600 of 1 and assayed for expression of myoXIa-CCT via western blot. Total extracted yeast protein was blotted using a myoXI-CCT antibody and ADH1 as a loading control. The condition MyoXIa-CCT V1422R+empty bait plasmid belongs to the western blot shown on the left but was rearranged for clarity.

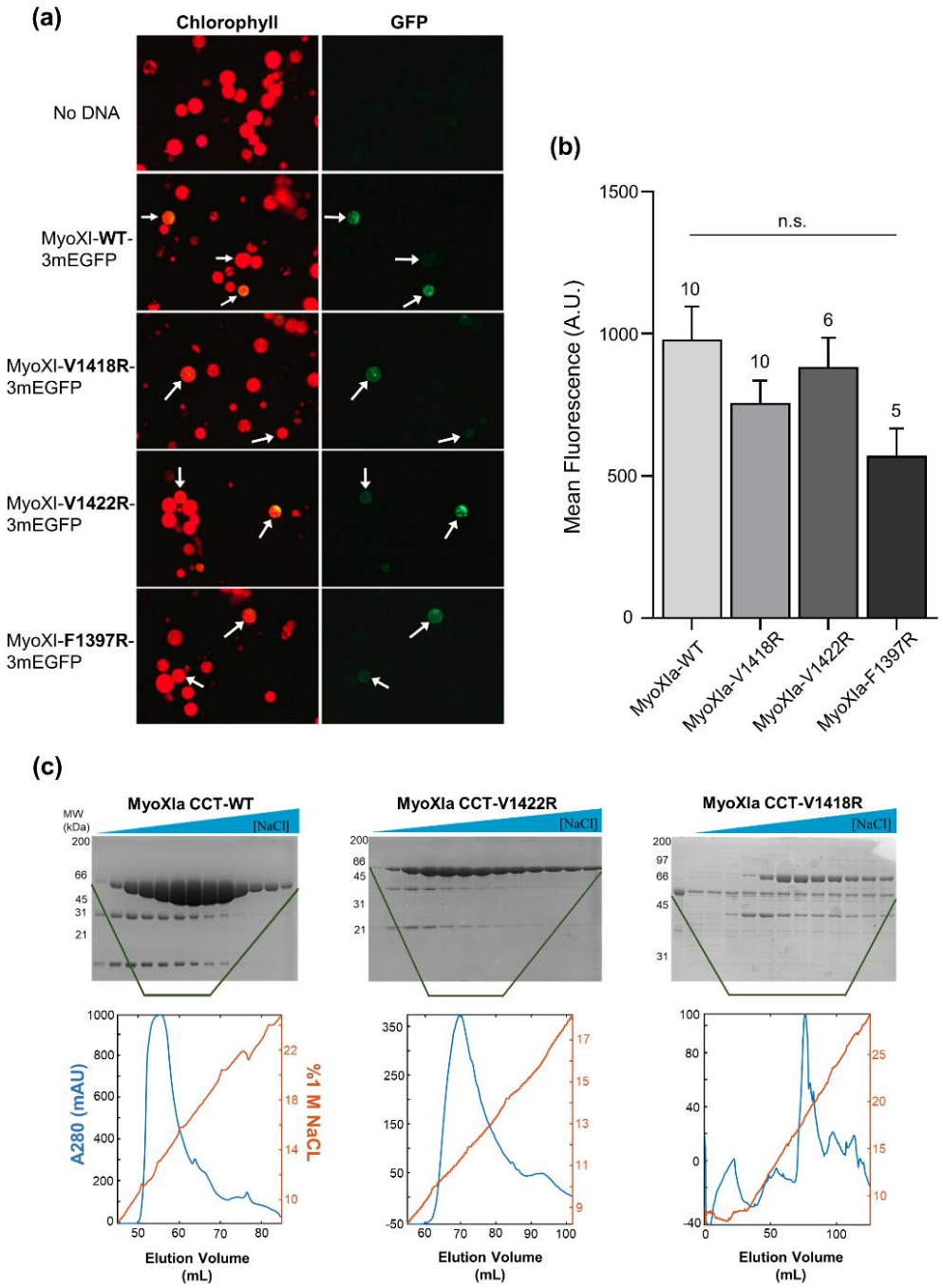

Fig. S8 Myosin XI cargo-binding domain mutants show varying levels of solubility. (a) Representative fluorescent images of wild-type moss protoplasts one day post-transformation with the indicated construct. (b) Quantification of expression for each fluorescent myosin XI fusion construct for images obtained in (a). Within a given condition, the mean fluorescence across all GFP positive protoplasts for a single independent transformation was treated as one sample. We plotted the mean of these independent sample means and failed to distinguish a statistically relevant difference, as tested by a one-way ANOVA ($P<0.05$). Error bars indicate the standard error of the mean and numbers above the SEM indicate the number of independent experiments. (c) SDS-PAGE gels of the elution fractions for WT and mutant myosin XI proteins following anion exchange chromatography. Each lane of the SDS-PAGE corresponds to fractions eluted from the column, with the absorbance at 280nm and percentage of 1 M NaCl plotted below.

Table S1 Primers used in this study.

Primer Name	Primer Sequence	Entry clone	Use
AttB1 Myo Head Neck For	GGGGACAAGTTTGTACAAAAAAGCAGGCTTAATGGCGACAGCAGGGAATGTA	pL1-MyoHeadNeck-R5	Phenotype/Complementation
AttB5r Myo Head Neck Rev	GGGGACAACTTTTGTATACAAAGTTGTACCCTTGGTCGGTGACAATAC	pL1-MyoHeadNeck-R5	Phenotype/Complementation
AttB5 Myo CC Tail For	GGGGACAACTTTGTATACAAAAGTTGTGTTGTCGAATCGATTCAAAAGCACCG	pL5-MyoCCTail-L2	Phenotype/Complementation
AttB2 Myo CC Tail Rev	GGGGACCACTTTGTACAAGAAAGCTGGGTACTAAGAATCTGGTTGTGG	pL5-MyoCCTail-L2	Phenotype/Complementation
AttB1 Myo Head Neck CC For	GGGGACAAGTTTGTACAAAAAAGCAGGCTTAATGGCGACAGCAGGGAATGTA	pL1-MyoHeadNeckCC-R5	Phenotype/Complementation
AttB5r Myo Head Neck CC Rev	GGGGACAACTTTTGTATACAAAGTTGTCAAAGAGTCTTGATTCTCCTGCT	pL1-MyoHeadNeckCC-R5	Phenotype/Complementation
AttB5 Myo Tail For	GGGGACAACTTTGTATACAAAAGTTGTGCTGCAATGTGTCATGCAAGAT	pL5-MyoTail-L2	Phenotype/Complementation
AttB2 Myo Tail Rev	GGGGACCACTTTGTACAAGAAAGCTGGGTACTAAGAATCTGGTTGTGG	pL5-MyoTail-L2	Phenotype/Complementation
Myo F1379R For	CGTGAGTGTTGCTCACGTAGCAACGGAGAGTAT	pL5-MyoTailF1379R-L2	Phenotype/Complementation
Myo F1379R Rev	TCTCAGCAGCAAACTGTTGAACAGCTGAACATT	pL5-MyoTailF1379R-L2	Phenotype/Complementation
Myo V1418R For	TATATCCGACAAGCACGTGGATTTTTGGTCATTCATC	pL5-MyoTailV1418R-L2	Phenotype/Complementation/Purification
Myo V1418R Rev	CTTGAGCTCATCCCATGACGCTCCAGCATACTC	pL5-MyoTailV1418R-L2	Phenotype/Complementation/Purification
Myo V1422R For	GCAGTTGGATTTTTGCGCATTCATCAAAAGCCA	pL5-MyoTailV1422R-L2	Phenotype/Complementation/Purification
Myo V1422R Rev	TTGTCGGATATACTTGAGCTCATCCCATGACGCTCC	pL5-MyoTailV1422R-L2	Phenotype/Complementation/Purification
Myo W1408R For	TATGCTGGAGCGTCACGGGATGAGCTCAAGTAT	pL5-MyoTailW1408R-L2	Phenotype/Complementation

Myo W1408R Rev	CTCCTCCCCAGCTTCATAAATCCAGTGCTCTAGTTCTG	pL5-MyoTailW1408R-L2	Phenotype/Complementation
Myo Y1384R For	TTTAGCAACGGAGAGCGTGTGAAAGCTGGACTT	pL5-MyoTailY1384R-L2	Phenotype/Complementation
Myo Y1384R Rev	TGAGCAACACTCACGTCTCAGCAGCAAACTGTT	pL5-MyoTailY1384R-L2	Phenotype/Complementation
MyoXIa-CCT WT For	CGCGGATCCGTTGTCGAATCGATTCAAAAGC	n/a	BamHI site for cloning into pETDuet/Purification
MyoXIa-CCT WT Rev	CCCAAGCTTCTAAGAATCTGGTTGTGGCATTAG	n/a	HindIII site for cloning into pETDuet/Purification
AttB2-PpRabE12 Rev	GGGGACCACTTTGTACAAGAAAGCTGGGTACTACGAGCAGCAGGAACTAGA	pL5-RabE12-pL2	Subcellular localization of RabE12/3xmEGFP tagging
AttB5-PpRabE12 For	GGGGACAACTTTGTATACAAAAGTTGTGATGGCCGCAGGTGGATCAAGA	pL5-RabE12-pL2	Subcellular localization of RabE12/3xmEGFP tagging
AttB5-PpRabE14 For	GGGGACAACTTTGTATACAAAAGTTGTGATGGCGACAAGAGCCC	pL5-RabE14-pL2	Subcellular localization of RabE14/3xmEGFP tagging
AttB5-PpRabE14 Rev	GGGGACCACTTTGTACAAGAAAGCTGGGTACTATGAGCAGCAAGAGCCAGA	pL5-RabE14-pL2	Subcellular localization of RabE14/3xmEGFP tagging
RabE11CDS_NotI_Forward	TAAGCAGCGGCCGCAATGGCCGCAGGTGGATC	y2hPrey-RabE11	RabE11 full-length in Y2H prey vector
RabE11CDS_BamHI_Reverse	TGCTTAGGATCCTCAAGAGCAACAGGAGCTACC	y2hPrey-RabE11	RabE11 full-length in Y2H prey vector
RabE15CDS_NotI_Forward	TAAGCAGCGGCCGCAATGGCGACAAGAGCTCGG	y2hPrey-RabE15	RabE15 full-length in Y2H prey vector
RabE15CDS_BamHI_Reverse	TGCTTAGGATCCCTATGAGCAGCAAGAGCCAGA	y2hPrey-RabE15	RabE15 full-length in Y2H prey vector
Y2Hprey_Forward	AATACCACTACAATGGAT	n/a	Sequencing primer for Y2H prey vector
Y2Hprey_Reverse	TCTAGACACTAGCTACTC	n/a	Sequencing primer for Y2H prey vector
RabE11i_Reverse	GGGGACCACTTTGTACAAGAAAGCTGGGTAGCTTGACCCTTCGCAGTGG	pL1-RabE11i-L2	Primer to amplify 401bp of RabE11 CDS for RNAi
RabE11i_Forward	GGGGACAAGTTTGTACAAAAAAGCAGGCTTAGATTACCTCATCAAGCTGCT	pL1-RabE11i-L2	Primer to amplify 401bp of RabE11 CDS for RNAi

RabE14_P2-F	AGTTTGGAGGGATGCTGAGTG	n/a	RabE14 CRISPR genotyping
RabE14_P2-R	GAGCCTGACCTTTGGCAAAAG	n/a	RabE14 CRISPR genotyping
RabE14_P1-F	TGCACATATTGCACAAACAGTCA	n/a	RabE14 CRISPR genotyping
RabE14_P1-R	AACATCACGTTCCTTCATTTCT	n/a	RabE14 CRISPR genotyping
RabE15_P2-F	CAGAGAGGCGGGTTTTGTAGT	n/a	RabE15 CRISPR genotyping
RabE15_P2-R	CCTCCGAAATGGTCCCAAGAA	n/a	RabE15 CRISPR genotyping
RabE15F_P1-F	CTAAGCCTTGCTAATGTAAACCA	n/a	RabE15 CRISPR genotyping
RabE15F_P1-R	ACAACGTTAGGTTAACAACACACT	n/a	RabE15 CRISPR genotyping
XIK-CCT_EcoRI For	TAAGCAGAATTCATGCTTTTACCGAGAACTCC	y2hBait-XIK CCT	*A. thaliana* XIK CCT Y2H bait vector
XIK-CCT_NotI Rev	TAAGCAGCGGCCGCTTACGATGTACTGCCTTCT	y2hBait-XIK CCT	*A. thaliana* XIK CCT Y2H bait vector
XIK-CCT_attB5	GGGGACAACTTTGTATACAAAAGTTGTGATGGCCACACGATCAAAAACA	pL5-XIK_CCT-L2	Creation of chimeric myosin XI with XI-K CCT
XIK-CCT_attB2	GGGGACCACTTTGTACAAGAAAGCTGGGTATTACGATGTACTGCCTTCTTTACG	pL5-XIK_CCT-L2	Creation of chimeric myosin XI with XI-K CCT
XIE-CCT_attB5	GGGGACAACTTTGTATACAAAAGTTGTGTTTCTCTCTGGCCGGTCC	pL5-XIE_CCT-L2	Creation of chimeric myosin XI with XI-E CCT
XIE-CCT_attB2	GGGGACCACTTTGTACAAGAAAGCTGGGTATTAGTCAGAACATGGCAATAGAAAG	pL5-XIE_CCT-L2	Creation of chimeric myosin XI with XI-E CCT
Ubi10-F	ACTACCCTGAAGTTGTATAGTTCGG	n/a	RT-qPCR
Ubi10-R	CAAGTCACATTACTTCGCTGTCTAG	n/a	RT-qPCR
E11_3prime_F	TGTGAAGCTGTCTGCTGGAG	n/a	RT-qPCR
E11_3prime_R	TTTCTGCCACCCAGCTTCAA	n/a	RT-qPCR
E12_3prime_F	GCCAGCTTCTAGTTCCTGCT	n/a	RT-qPCR
E12_3prime_R	CGCTCTCCCACTAACAGCTT	n/a	RT-qPCR
E13_3prime_F	AGGATGCCAAGCCAGATGTC	n/a	RT-qPCR
E13_3prime_R	AGCTCACCAGACCAATGTCG	n/a	RT-qPCR

Table S2 Gene IDs and source of protein sequences used in phylogenetic tree construction.

Name	Description	Sequence Length
Volvox carteri	Vocar.0012s0034.1 (Phytozome)	217
S.c. Ypt1	P01123 (Uniprot)	206
Coccomyxa subellipsoidea	26393 (Phytozome)	210
Chlamydomonas reinhardtii	Cre15.g641800.t1.2 (Phytozome)	183
H.s. Rab8a	P61006 (Uniprot)	207
A.t. RabE1E	At3g09900 (Phytozome-TAIR10)	218
A.t. RabE1D	At5g03520 (Phytozome-TAIR10)	216
A.t. RabE1B	AT5G59840 (Phytozome-TAIR10)	216
A.t. RabE1A	At3g53610 (Phytozome-TAIR10)	216
A.t. RabE1C	At3g46060 (Phytozome-TAIR10)	216
P.p. RabE15	Pp3c5_21410 (Phytozome-Pp v3.3)	215
P.p. RabE13	Pp3c25_7430 (Phytozome-Pp v3.3)	216
P.p. RabE14	Pp3c6_11710 (Phytozome-Pp v3.3)	215
P.p. RabE11	Pp3c16_17460 (Phytozome-Pp v3.3)	216
P.p. RabE12	Pp3c16_17470 (Phytozome-Pp v3.3)	216
S.c. Sec4	P07560 (Uniprot)	215

Methods S1. Experimental procedures for supplemental figures

Phylogenetic analyses

The full-length clone identified in our Y2H screen was categorized as Rab-E14 in accordance with its sequence agreement with the predicted cDNA of gene Pp3c6_11710 (*Physcomitrella patens* v3.3 (Lang et al., 2018)). We then used the predicted protein sequence and BLAST to analyze the *P.patens* proteome using Phytozome (http://phytozome.jgi.doe.gov), as well as *C. subellipsoidea*, *C. reinhardtii*, *V. carteri*, and *A. thaliana*, with an expectation threshold of E = 10^{-4} and BLOSUM62 substitution matrix. All hits were filtered to allow only putative Rab-E protein sequences for tree construction. We determined if a given sequence was a Rab-E using the "Rabifier" (rabdb.org) classification pipeline (Diekmann et al., 2011; Surkont et al., 2017) that predicts if the query sequence is a Rab, and if so, groups it into the most likely Rab subfamily based upon canonical subfamily sequence motifs (Pereira-Leal and Seabra, 2000). We added well-characterized Rab8 proteins Sec4 and Rab8a to observe eukaryotic divergence, as well as a known non-Rab8, Ypt1, to function as the outgroup. Sequences were aligned using MUSCLE (Edgar, 2004) under default parameters. The phylogenetic tree was constructed under the ML information criterion using PhyML (Guindon et al., 2010), model selection was performed using the Akaike Information Criterion (Akaike, 1974), and 100 bootstraps were executed for statistical branch support. This process was facilitated through use of the ATGC PhyML web server (Guindon et al., 2005). The sources of all sequences used for phylogenetic tree construction are found in Table S2.

Western blot analysis

Y2H strains were analyzed for MyoXIa-CCT expression by picking individual colonies from SD -trp -leu plates, growing to 1 OD600 unit, and extracting total protein via a NaOH and SDS-PAGE buffer treatment (Kushnirov, 2000). Total protein was run on a 12% SDS-PAGE gel, transferred to a PVDF membrane, cut, then blotted against myosin XI-CCT (1:10,000--~80kDa) using a custom-made antibody, and yeast ADH1 (1:1,000--~40kDa) (Abcam:ab34680) as a loading control. The myosin XIa-CCT antibody was generated against a 6xHis fusion of the myosin XIa-CCT (Capralogics, Inc. Hardiwick, MA).

Myosin XI protoplast expression

The mutant and WT myosin XIa expression constructs were reamplified with primers containing attB1 and attB5 sites (Table S1) to facilitate c-terminal tagging with three tandem copies of monomeric enhanced GFP (3mEGFP). Entry clones of myosin XI (WT and mutants) and 3mEGFP were cloned into a moss expression plasmid with LR clonase (Thermo Fisher), yielding pB1-MyoHNC-B5-gtail-*mutation*-B5-3mEGFP-B2. Constructs were transformed into moss protoplast as previously described (Vidali et al., 2007), except transformed protoplasts were left in suspension in liquid plating medium, instead of being cultured on solid medium.

One day post-transformation, protoplasts were removed from the growth chamber and centrifuged at 250 *g* for five minutes. The supernatant was removed, such that 1ml remained, and the protoplasts were

gently resuspended. Slides for imaging were prepared by affixing an approximately 22x22mm square of Parafilm, with a circle cut out of the center, to a glass microscope slide using heat. Approximately 65 µl of protoplasts were transferred to the circle bounded by Parafilm on the slide, then sealed with a 22x22mm glass coverslip. Images of fluorescent protoplasts were acquired using the same equipment described by Bibeau and Vidali (Bibeau and Vidali, 2014).

In brief, protoplasts were imaged using three separate filters: chlorophyll channel (480/40 bandpass excitation filter, 505 longpass dichroic, 510 longpass emission); standard GFP filter (for GFP expression); standard dsRed filter (dead cells/background subtraction). All three images were imported into ImageJ, contrast enhanced, then the dsRed signal was subtracted from the GFP channel to avoid quantification of dead protoplasts. The red channel was used to visualize the protoplast morphology and was manually segmented using the magic wand tool and ROI manager. The mean gray values for all ROIs were measured on the GFP channel and exported. All fluorescent values were filtered based on the fluorescence of the "no DNA" condition—the maximum value obtained within the "no DNA" condition was used as a threshold for all other conditions for that respective day to discard untransformed or non-expressing protoplasts. The remaining values were averaged by date of transformation for each condition and tested for statistical differences.

References for Supporting Information

Akaike, H. (1974). A new look at the statistical model identification. IEEE Trans. Autom. Control **19,** 716-723.

Bibeau, J.P., and Vidali, L. (2014). Morphological analysis of cell growth mutants in *Physcomitrella*. Methods Mol Biol **1080,** 201-213.

Diekmann, Y., Seixas, E., Gouw, M., Tavares-Cadete, F., Seabra, M.C., and Pereira-Leal, J.B. (2011). Thousands of rab GTPases for the cell biologist. PLoS Comput Biol **7,** e1002217.

Edgar, R.C. (2004). MUSCLE: multiple sequence alignment with high accuracy and high throughput. Nucleic Acids Res. **32,** 1792-1797.

Guindon, S., Lethiec, F., Duroux, P., and Gascuel, O. (2005). PHYML Online--a web server for fast maximum likelihood-based phylogenetic inference. Nucleic Acids Res. **33,** W557-559.

Guindon, S., Dufayard, J.F., Lefort, V., Anisimova, M., Hordijk, W., and Gascuel, O. (2010). New algorithms and methods to estimate maximum-likelihood phylogenies: assessing the performance of PhyML 3.0. Syst. Biol. **59,** 307-321.

Lang, D., Ullrich, K.K., Murat, F., Fuchs, J., Jenkins, J., Haas, F.B., Piednoel, M., Gundlach, H., Van Bel, M., Meyberg, R., Vives, C., Morata, J., Symeonidi, A., Hiss, M., Muchero, W., Kamisugi, Y., Saleh, O., Blanc, G., Decker, E.L., van Gessel, N., Grimwood, J., Hayes, R.D., Graham, S.W., Gunter, L.E., McDaniel, S.F., Hoernstein, S.N.W., Larsson, A., Li, F.W., Perroud, P.F., Phillips, J., Ranjan, P., Rokshar, D.S., Rothfels, C.J., Schneider, L., Shu, S., Stevenson, D.W., Thummler, F., Tillich, M., Villarreal Aguilar, J.C., Widiez, T., Wong, G.K., Wymore, A., Zhang, Y., Zimmer, A.D., Quatrano, R.S., Mayer, K.F.X., Goodstein, D., Casacuberta, J.M., Vandepoele, K., Reski, R., Cuming, A.C., Tuskan, G.A., Maumus, F., Salse, J., Schmutz, J., and Rensing, S.A. (2018). The *Physcomitrella patens* chromosome-scale assembly reveals moss genome structure and evolution. Plant J **93,** 515-533.

Pereira-Leal, J.B., and Seabra, M.C. (2000). The mammalian Rab family of small GTPases: definition of family and subfamily sequence motifs suggests a mechanism for functional specificity in the Ras superfamily. J. Mol. Biol. **301,** 1077-1087.

Surkont, J., Diekmann, Y., and Pereira-Leal, J.B. (2017). Rabifier2: an improved bioinformatic classifier of Rab GTPases. Bioinformatics **33,** 568-570.

Vidali, L., Augustine, R.C., Kleinman, K.P., and Bezanilla, M. (2007). Profilin is essential for tip growth in the moss *Physcomitrella patens*. Plant Cell **19,** 3705-3722.